UNIVERSAL WISER
PUBLISHER

Research Article

Study on Glyphosate Adsorption onto ZIF-8 Modified with Fe_3O_4 Nanoparticles

Immanuel Joseph Ondang[1], Kuan-Chen Cheng[2,3,4,5], Alchris Woo Go[6], Artik Elisa Angkawijaya[7], Shella Permatasari Santoso[1,8*] [ID]**, Felycia Edi Soetaredjo[1,8], Suryadi Ismadji[1,8], Hsien-Yi Hsu[9,10], Chang-Wei Hsieh[11,12], Phuong Lan Tran-Nguyen[13]**

[1] Chemical Engineering Department, Faculty of Engineering, Widya Mandala Surabaya Catholic University, Kalijudan 37, Surabaya 60114, Indonesia
[2] Institute of Food Science and Technology, National Taiwan University, #1, Sec. 4, Roosevelt Rd., Taipei 10617, Taiwan
[3] Institute of Biotechnology, National Taiwan University, #1, Sec. 4, Roosevelt Rd., Taipei 10617, Taiwan
[4] Department of Medical Research, China Medical University Hospital, China Medical University, 91, Hsueh-Shih Road, Taichung 40402, Taiwan
[5] Department of Optometry, Asia University, 500, Lioufeng Rd., Wufeng, Taichung 41354, Taiwan
[6] Department of Chemical Engineering, National Taiwan University of Science and Technology, No. 43, Sec. 4, Keelung Rd, Da'an District, Taipei City 10607, Taiwan
[7] Center for Sustainable Resource Science, RIKEN, Yokohama 230-0045, Japan
[8] Collaborative Research Center for Sustainable and Zero Waste Industries, Kalijudan 37, Surabaya 60114, East Java, Indonesia
[9] School of Energy and Environment, Department of Materials Science and Engineering, City University of Hong Kong, Kowloon Tong, Hong Kong, China
[10] Shenzhen Research Institute, City University of Hong Kong, Shenzhen 518057, China
[11] Department of Food Science and Biotechnology, National Chung Hsing University, South Dist., Taichung City 40227, Taiwan
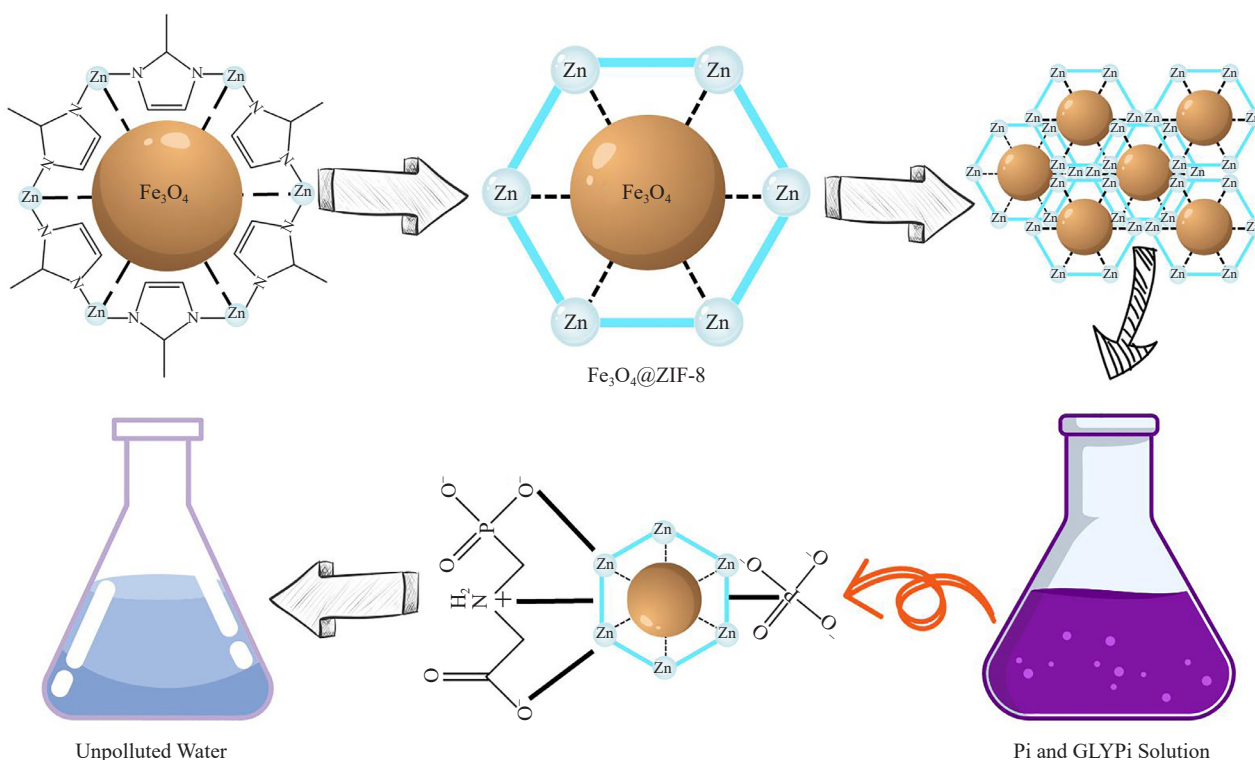[12] Department of Medical Research, China Medical University Hospital, North Dist., Taichung City 404333, Taiwan
[13] Faculty of Mechanical Engineering, Can Tho University, Can Tho, Vietnam
 Email: shella@ukwms.ac.id

Fe₃O₄@ZIF-8

Unpolluted Water

Pi and GLYPi Solution

Abstract: Glyphosate (GLYPi) is an organophosphorus herbicide that behaves as an anionic substance in the aqueous phase. Even though it is stated as safe and non-toxic, the widespread use of GLYPi has raised environmental issues that need attention. This work used the positively charged metal-organic framework (MOF) of ZIF-8 to remove GLYPi via adsorption. Fe_3O_4 particles were hybridized with ZIF-8 to obtain Fe_3O_4@ZIF-8 via an *in-situ* deposition strategy to enhance the adsorption capacity toward GLYPi. The composite material (Fe_3O_4@ZIF-8) was characterized using scanning electron microscopy, Fourier transform infrared spectroscopy, and X-ray diffraction, revealing rhombic dodecahedron-shaped particles and oxygen-rich functional groups. The adsorption results show that there is a synergistic effect of adding Fe_3O_4 to ZIF-8 in increasing the rate and capacity of adsorption on GLYPi, that is 0.0012 g/mg·min (Pseudo-second-order) and 73.57 mg/g (Langmuir), respectively, on pH 7 and 50 °C. GLYPi adsorption by Fe_3O_4@ZIF-8 was not influenced by coexisting anions (e.g., Cl^-, NO_3^-, SO_4^{2-}, and HCO_3^-). The reusability study showed that the adsorption efficiency of GLYPi by Fe_3O_4@ZIF-8 decreased significantly after the first cycle, which should be considered a future challenge for further studies. The adsorption mechanisms of GLYPi by Fe_3O_4@ZIF-8 involve electrostatic interaction and pore-filling. The results indicate that Fe_3O_4@ZIF-8 is a promising candidate for removing organophosphate compounds, which could be an excellent strategy for environmental protection.

Keywords: adsorption, glyphosate, ZIF-8, Fe_3O_4, phosphate herbicide

1. Introduction

Using herbicides to control weed growth has become a common practice to increase crop yields. Glyphosate (GLYPi), an organophosphate compound also called N-phosphonomethyl glycine, is a non-selective herbicide that has been commercialized since 1974.[1-2] GLYPi is a systemic herbicide with broad-spectrum activity, working by inhibiting plant enzymes that responsible for the synthesis of amino acid.[1] In the earlier stages of commercialization, GLYPi was introduced as a non-toxic and biodegradable herbicide.[3] Following the statement, GLYPi has developed into one of

agriculture's most frequently used herbicides. Annual use of GLYPi increased exponentially from 56,000 tons in 1994 to 825,000 tons in 2014. GLYPi has also been widely used as an active ingredient blend for > 750 broad-spectrum herbicide varieties.[4]

Extensive use of GLYPi has raised concerns regarding the potential environmental damage and resulting health hazards.[5-6] As research and technology advances, many studies refute the safety of GLYPi. GLYPi is a stable compound that can last several months in dark environmental conditions without experiencing degradation.[1,3] Furthermore, GLYPi contains three deprotonable functional groups with acid dissociation constant (pKa) values of 2.2 for the carboxylate (-COOH), 5.5 for the phosphonate (-PO_3H_2), and 10.2 for the amine (-NH_2) group.[7] Due to these deprotonate groups, GLYPi is extremely soluble in water,[8] increasing the possibility of its environmental exposure. GLYPi residues in the soil can also cause phytotoxicity in non-target plants through root uptake, which can cause biodiversity loss.[8] Apart from that, the use of GLYPi also increases the total phosphorous content in the soil and surrounding surface water, which can trigger eutrophication.[9] Highlighting the potential damage caused by GLYPi, this study offers a breakthrough in managing GLYPi contamination in the aqueous phase.

Methods for reducing or eliminating harmful substances in the aqueous phase have become a hot topic in materials and environmental science. Adsorption is one of the most promising techniques in water treatment for various hazardous substances because of its low operating cost, practicality, high efficiency, and ease of adaptation to multiple substances.[10] The adsorption procedure involves using a solid material (sorbent) as a medium for the attachment of target molecules (sorbates). The deprotonable nature of GLYPi allows it to exist as negatively charged molecules in the aqueous phase. Waters generally have a pH between 6.5 and 8.5; GLYPi is presented as an anionic species over this range of pH.[11] Therefore, using positively charged sorbents can create electrostatic attraction towards negatively charged GLYPi.

The use of metal-organic frameworks (MOFs) as adsorbents has attracted extensive research interest due to their superior adsorption capacity owing to large specific surface area, high porosity, and diverse functionality. In particular, the zeolitic imidazolate framework (ZIF-8) has been mentioned for its superior chemical and thermal stability among other MOFs owing to its zeolitic structure.[12] ZIF-8 also exhibits a positive surface charge, which makes it an excellent candidate for the adsorption of anionic sorbates, such as phosphate (PO_4^{3-}),[13] Congo red,[14] dimethyl methyl phosphonate,[12] hexavalent chromium,[15] etc. Of the many adsorption studies using ZIF-8 as a sorbent, there is still no study demonstrating the adsorption performance of ZIF-8 on GLYPi.

GLYPi is commonly found to coexist with various anions in wastewater; therefore, an adsorbent with high selectivity is often required to remove it effectively. Pearson's hard-soft acid-base theory states that Fe is a hard acid that can establish strong bonds with hard bases, including phosphonate-containing molecules.[16-18] Therefore, incorporating Fe-containing materials into ZIF-8 could be a good strategy to increase its affinity for GLYPi. Fe_3O_4 magnetic particles are combined with ZIF-8 for this purpose. This work revealed the performance of ZIF-8 and Fe_3O_4@ZIF-8 adsorbent for removing GLYPi through adsorption isotherms and kinetics study. Additionally, at the end of the work, the adsorption performance of the adsorbents on phosphate (Pi) was also evaluated as a comparison. The two compounds GLYPi and Pi exhibit chemical resemblance; thus, the adsorbent may show similar adsorption performance toward both compounds. Furthermore, Pi is also known to raise eco-toxicological concerns because of its potential to cause eutrophication.

2. Materials and method
2.1 *Materials*

The chemicals used in this work including zinc nitrate hexahydrate ($Zn(NO_3)_2 \cdot 6H_2O$, CAS 10196-18-6, 98% purity), 2-methylimidazole (CAS 693-98-1, 99% purity), sodium hydroxide (NaOH, CAS 1310-73-2; ≥ 98.5% purity), sulfuric acid (H_2SO_4, CAS 7664-93-9, 96% purity), ammonium heptamolybdate tetrahydrate (($NH_4)_6Mo_7O_{24} \cdot 4H_2O$, CAS 12054-85-2), antimony potassium tartrate trihydrate ($C_8H_6K_2O_{13}Sb_2 \cdot 3H_2O$, CAS: 28300-74-5), L-ascorbic acid ($C_6H_8O_6$, CAS 50-81-7, ≥ 99% purity), sodium molybdate (Na_2MoO_4, CAS 7631-95-0, ≥ 9 8.0% purity), ninhydrin ($C_9H_6O_4$, ACS Reagent Grade, CAS 485-47-2), potassium phosphate (KH_2PO_4, CAS 7778-77-0, ≥ 99.0% purity), and glyphosate (GLYPi, $(HO)_2P(O)CH_2NHCH_2CO_2H$, CAS 1071-83-6, 96% purity). All chemicals were acquired from Sigma Aldrich, Singapore, and utilized without further purification.

2.2 Adsorbent preparation

2.2.1 Preparation of ZIF-8

ZIF-8 was synthesized following the procedure by Jian et al.[19] The 2-methylimidazole solution was prepared by dissolving 4.54 g (0.055 mol) of the compound in 40 mL of distilled water. In a separate beaker, 0.29 g (0.001 mol) $Zn(NO_3)_2 \cdot 6H_2O$ was dissolved in 20 mL of distilled water. The two solutions were mixed and reacted for 24 h at room temperature. The ZIF-8 solid precipitate was then collected and washed thrice using ethanol and dried in an oven at 80 °C overnight.

2.2.2 Preparation of Fe_3O_4

The ferric solution was prepared by mixing 0.016 mol $FeCl_3 \cdot 6H_2O$ and 0.008 mol $FeCl_2.4H_2O$ in 80 mL of water. The solution was stirred continuously and heated to 70 °C before adding 20 mL of 25% (w/w) ammonia solution. The mixture was allowed to react for 30 min at 70 °C. Subsequently, 4 mL of 0.5% (w/v) of citric acid solution was added to the mixture, then the temperature was increased to 90 °C and the mixture was reacted for 60 min. The precipitate formed was collected and washed with water five times. The collected solids were then resuspended in water, and an external magnetic field was applied to separate the magnetic and non-magnetic particles. The magnetic particles were collected and dried under a vacuum at room temperature.

2.2.3 Preparation of composite Fe_3O_4@ZIF-8

4 mL of Fe_3O_4 suspension in water was prepared at different 1 to 5 mg/mL concentrations. A 2-methylimidazole solution (4.54 g in 36 mL of water) was added to the Fe_3O_4 suspension while sonicating. The mixture was sonicated for 15 min before adding $Zn(NO_3)_2 \cdot 6H_2O$ solution (0.29 g in 20 mL of water). The final content of Fe_3O_4 in the mixture is summarized in Table 1. The mixture was then reacted for 24 h at room temperature to allow the formation and deposition of ZIF-8 on Fe_3O_4. The forming solid was separated using an external magnetic field, washed using ethanol three times, and dried in an 80 °C oven overnight.

Table 1. Composition of starting materials in preparing the Fe_3O_4@ZIF-8 composite

Fe_3O_4		2-Methylimidazole		$Zn(NO_3)_2 \cdot 6H_2O$		Fe_3O_4 content (% w/v)*
Mass (mg)	Vol. (mL)	Mass (g)	Vol. (mL)	Mass (g)	Vol. (mL)	
0	4	4.54	66	0.29	10	0
4	4	4.54	66	0.29	10	5.7
8	4	4.54	66	0.29	10	11.4
12	4	4.54	66	0.29	10	17.1
16	4	4.54	66	0.29	10	22.9
20	4	4.54	66	0.29	10	28.6

* Fe_3O_4 content was calculated from the ratio of mass Fe_3O_4 added and the total volume of the system

The amount of Fe_3O_4 in the resultant composite was evaluated by determining the Fe content, and the determination was performed using an atomic absorption spectroscopy procedure on a Shimadzu AA-6200 spectrophotometer. The Fe

content (%) was calculated according to the following eq. (1).

$$\text{Fe content } (\%) = \frac{\text{Conc. of Fe detected (mg/L)}}{\text{mass of Fe}_3\text{O}_4\text{(mg)}} \times \text{Vol. sample (L)} \times 100\% \qquad (1)$$

2.3 Characterization

X-ray diffraction (XRD) analysis to elucidate the crystallinity pattern of the sample was carried out using a Bruker D2 Phaser diffractometer, with Cu Kα X-ray source at λ of 1.5418 Angstrom operated at 30 kV and 10 mA, and detection range at 2θ of 5° to 50°. The surface functional groups were determined through the Fourier transform infrared (FTIR) spectroscopy method using a Shimadzu 8400S spectrometer; detection was performed from a wavenumber of 400 to 4,000 cm^{-1}. Nitrogen (N$_2$) sorption isotherm analysis was performed using a Micromeritics ASAP 2020 analyzer, and the sample was degassed for 12 h at 200 °C before the analysis. The pH drift method was carried out to determine the point-of-zero-charge (PZC)[20-21] -15 mg of adsorbent was immersed in a 0.01 M NaCl solution, which was prepared at various pH of 2 to 12; the pH adjustment was done by adding NaOH or HCl. After 48 h of immersion, the final pH was measured using a calibrated pH meter. The initial pH vs. final pH graph was then plotted to determine the PZC value.

2.4 Adsorption experiment

2.4.1 Adsorption kinetics

Adsorption kinetics was performed in batch experiment. A 25 mL GLYPi solution was prepared at a concentration of 20 mg/L, and then 15 mg of selected adsorbent was introduced into the solution. The adsorption was performed in a thermostatted shaker water bath (Memmert) at a temperature of 30 °C. The residual concentration of GLYPi was measured at a designated period between 0 to 300 min. The kinetic analysis was also performed for GLYPi at 40 and 60 mg/L concentrations.

2.4.2 Adsorption isotherm

Adsorption isotherm study was carried out by introducing 15 mg of selected adsorbent into a 25 mL GLYPi solution prepared at various initial concentrations from 0 to 120 mg/L. The adsorption was performed for 6 h at three different temperatures of 303, 313, and 323 K (30, 40, and 50 °C) in a thermostatted shaker water bath (Memmert).

2.4.3 Effect of operating conditions

The effect of pH in the adsorption process was investigated. A series of 25 mL GLYPi solution at a concentration of 40 mg/L was prepared. The pH of the solution was adjusted in the range of 3 to 10 by using 0.1 M HCl or 0.1 M NaOH solution. Then, 15 mg of adsorbent was introduced, and the residual GLYPi was measured after 6 h.

The effect of coexisting ions was investigated by performing the adsorption in a solution containing different types of salt, that is, NaCl, Na$_2$SO$_4$, NaNO$_3$, and NaHCO$_3$. Specifically, 40 mg/L of GLYPi solution was prepared in 25 mL of 15 mM salt solution. Then, 15 mg of selected adsorbent was introduced, and the adsorption was performed for 6 h.

2.4.4 Colorimetric measurement of GLYPi concentration

To determine the amount of residual GLYPi in bulk solution, 2 mL of GLYPi-containing sample was mixed with 1 mL of 5 wt.% of sodium molybdate solution and 1 mL of 2 wt.% ninhydrin solution. The mixture was mixed and heated in a water bath at 100 °C for 20 min. The solution was allowed to cool down until the "Ruhemann" purple color formed. Subsequently, the solution was transferred into a measuring flask, and water was added to the solution to make a final volume of 10 mL. The absorbance of the sample was measured using a spectrophotometer at a wavelength of 570 nm. The removal efficiency (%) was calculated according to eq. (2).

$$\text{Removal efficiency (\%)} = \frac{C_0 - C_f}{C_0} \times 100 \tag{2}$$

where C_0 and C_f represent the initial and final concentration of GLYPi (mg/L), respectively. The amount of solute at a particular time (Q_t) or at equilibrium (Q_e) was calculated using eq. (3).

$$Q_t \text{ or } Q_e \text{ (mg/g)} = \frac{C_0 - (C_t \text{ or } C_e)}{m} \times V \tag{3}$$

where C_t is the concentration at a particular time (mg/L), C_e is the concentration at equilibrium (mg/L), m is the mass of adsorbent (g), and V is the total volume of solution (L).

2.5 *Reusability study*

The used adsorbent was regenerated by stirring the adsorbent in 50 mL of 0.05 M ethanolic NaOH solution for 15 min at room temperature. The regenerated adsorbent was then reused for another batch of adsorption experiments.

3. Results and discussion

3.1 *Effect of Fe₃O₄ addition on the GLYPi removal efficiency*

Fe$_3$O$_4$@ZIF-8 composite was prepared by mixing a varied amount of Fe$_3$O$_4$. The amount of Fe$_3$O$_4$ added affects the Fe content in the composite, as shown in Figure 1a. Using a higher amount of Fe$_3$O$_4$ resulted in a higher Fe content in the composite. The effect of Fe$_3$O$_4$ addition in enhancing the removal efficiency of Fe$_3$O$_4$@ZIF-8 composite against GLYPi was shown in Figure 1b; this result also set as a preliminary trial to determine the optimal amount of Fe$_3$O$_4$ in producing adsorbent with excellent removal efficiency. As shown in Figure 1b, the removal efficiency of GLYPi is increased with the increase of Fe$_3$O$_4$ amount from 0 to 17 %w/v. However, adding Fe$_3$O$_4$ of > 17 %w/v does not significantly improve removal efficiency. The result of the preliminary trial indicates that the addition of 17 %w/v Fe$_3$O$_4$ produces Fe$_3$O$_4$@ZIF-8 composite with optimum GLYPi removal efficiency; thus, the following results and discussion are carried out using the respective adsorbent composite.

3.2 *Adsorbent characterization*

3.2.1 *Point-of-zero charge*

Point-of-zero-charge (PZC) is a pH-dependent property that significantly affects adsorption performance.[22-23] The pH drift method is used to determine PZC, which is one of the robust and facile methods to determine PZC.[20] As shown from the measurement result in Figure 1c, ZIF-8 and Fe$_3$O$_4$@ZIF-8 exhibit similar PZC values 8.8 as indicated by the intersection point (Figure 1c). The pH difference value (ΔpH) value is also plotted to depict the pH distribution at which the adsorbent has a positive surface charge (positive ΔpH) and at which the adsorbent has a negative surface charge (negative ΔpH). The plot is shown in Figure 1d. It can be noted that the adsorbent shows a positive ΔpH at pH environment < PZC, and a negative ΔpH at pH environment > PZC. Thus, it can be expected that the removal of negatively charged GLYPi molecules occurs at a higher rate when the pH < 8.8, when the adsorbent is positively charged.
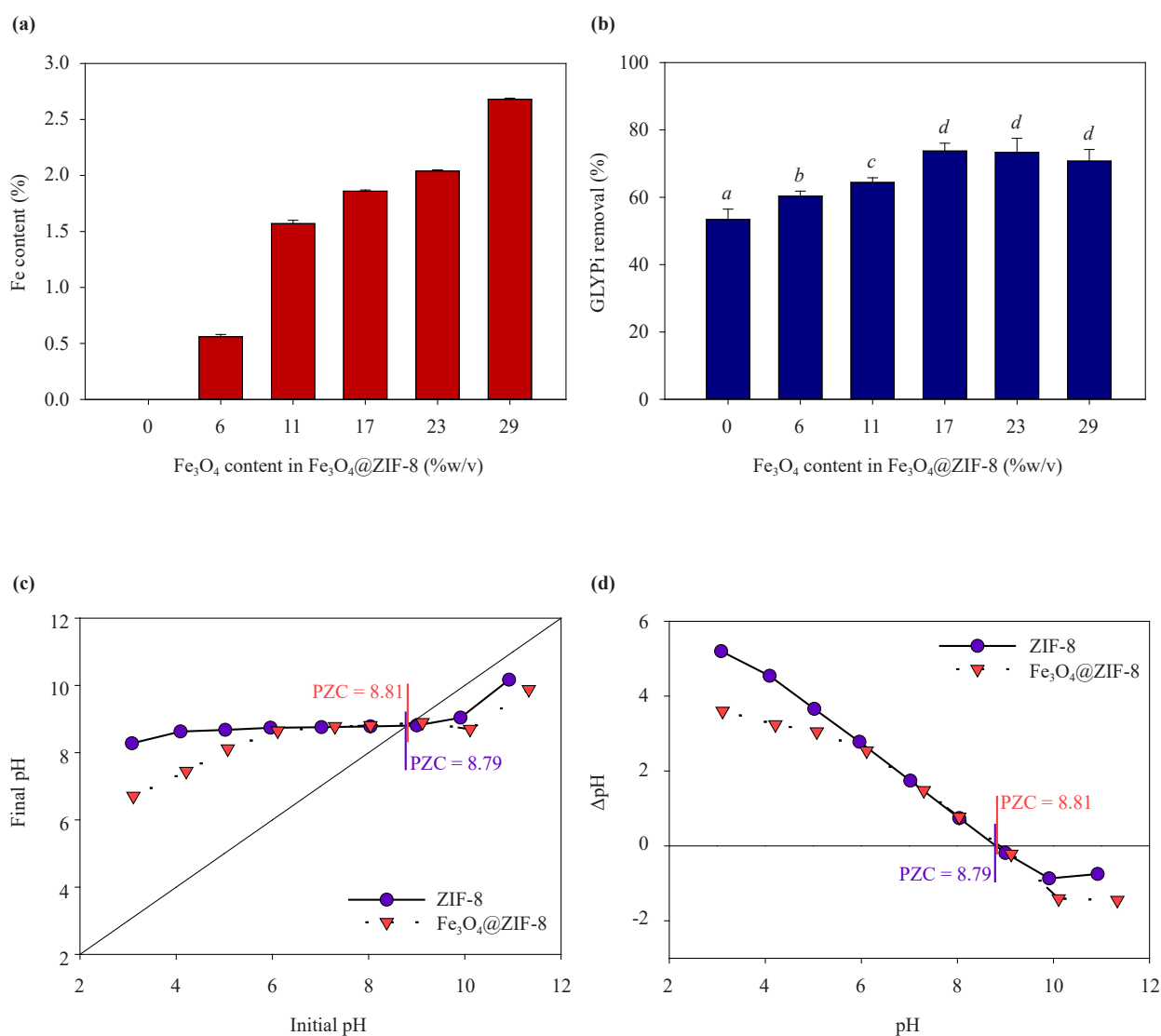
Figure 1. (a) The variation of Fe content and (b) GLYPi removal efficiency of Fe_3O_4@ZIF-8 composite prepared using different amounts of Fe_3O_4; different lowercase letters indicate significant differences with *p*-value < 0.05. (c) Point-of-zero-charge and (d) ΔpH value of ZIF-8 and Fe_3O_4@ZIF-8 prepared using 17 %w/v of Fe_3O_4

3.2.2 *SEM analysis*

SEM analysis was performed to elucidate the particle morphology and surface characteristics of the investigated materials, which are ZIF-8, Fe_3O_4, and Fe_3O_4@ZIF-8. The rhombic dodecahedron shape of the ZIF-8 particle is shown in Figure 2a. The Fe_3O_4 particle morphology is shown in Figure 2b; the formation of large particles suggests the presence of aggregation. The morphology of the Fe_3O_4@ZIF-8 composite is shown in Figure 2c, and the particles exhibit a morphology similar to that of ZIF-8. However, it can be seen that the Fe_3O_4@ZIF-8 particles have a rougher surface due to the anchoring of ZIF-8 onto Fe_3O_4. The elemental mapping of Fe_3O_4@ZIF-8 indicates the presence of Zn and Fe elements, which confirms the successful hybridization of the ZIF-8 and Fe_3O_4.
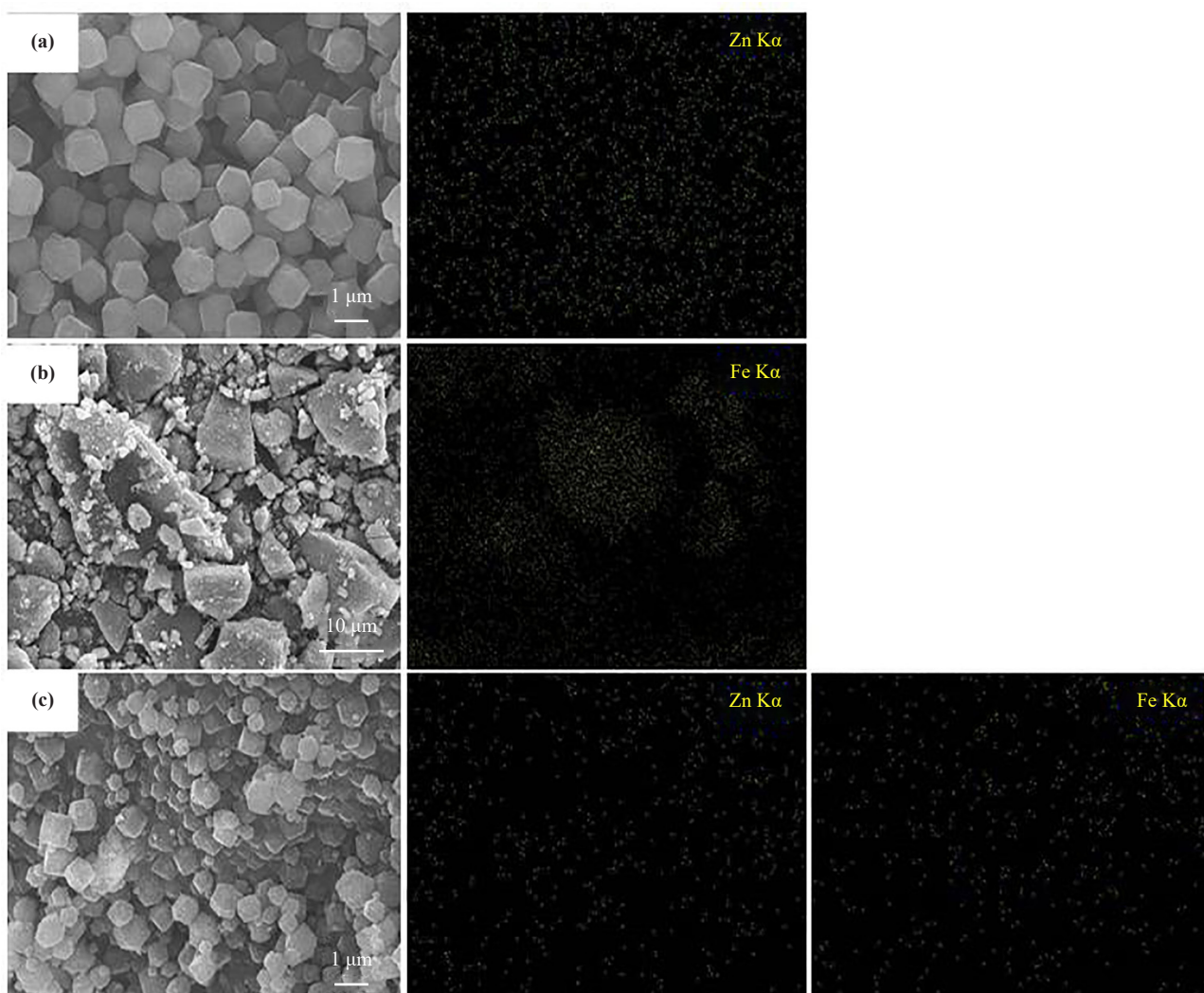
Figure 2. SEM morphology and EDX elemental mapping of (a) ZIF-8, (b) Fe_3O_4, and (c) Fe_3O_4@ZIF-8

3.2.3 *XRD analysis*

XRD crystallinity pattern and the corresponding crystal plane of ZIF-8, Fe_3O_4, and Fe_3O_4@ZIF-8 are shown in Figure 3. The ZIF-8 exhibits peaks at 2θ of 7.4°, 10.6°, 12.7°, 15.0°, 16.4°, and 18.1° corresponding to crystal plane of (011), (002), (112), (022), (013), and (222), which are in good agreement with the reported ZIF-8 by Guo et al.[24] Other peaks correlated to the formation of ZIF-8 were also observed at $2\theta > 22$°, which are similar to the reported literature.[25-26] For Fe_3O_4, typical diffraction peaks corresponding to (220), (311), (222), (400), and (422) planes are identified at 30.3°, 35.8°, 37.5°, 43.5°, and 53.8°, respectively. The corresponding composite of Fe_3O_4@ZIF-8 exhibits a similar XRD pattern to that of ZIF-8, where almost all ZIF-8 peaks can be detected but at a lower intensity. The detection of the ZIF-8-correlated peaks in the XRD of Fe_3O_4@ZIF-8 also implies that the ZIF-8 crystal structure is not being destroyed.

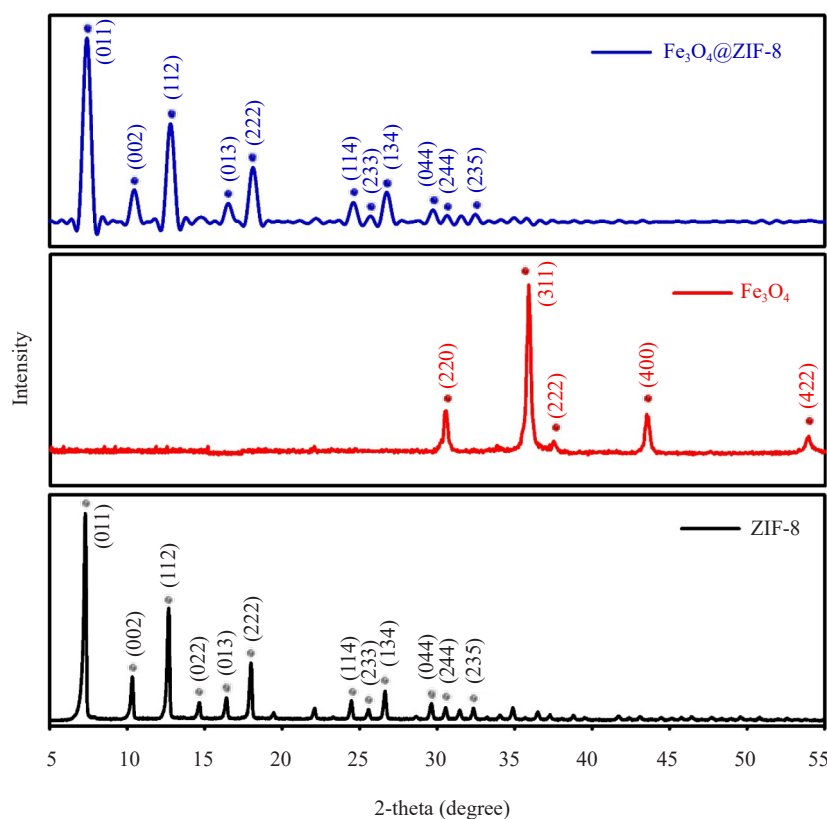**Figure 3.** XRD pattern of ZIF-8, Fe$_3$O$_4$, and Fe$_3$O$_4$@ZIF-8

3.2.4 *FTIR analysis*

The functional groups of ZIF-8, Fe$_3$O$_4$, and Fe$_3$O$_4$@ZIF-8 were examined using FTIR analysis, and the result is provided in Figure 4. As observed from the spectra of ZIF-8, the presence of aromatic and aliphatic stretching vibration of C-H groups of imidazole was noted from the absorption bands at 2,845 and 3,183 cm^{-1}, respectively. The stretching vibration of C = N was presented from the band at wavenumber 1,603 cm^{-1}. The band occurs at a wavenumber of 1,451 cm^{-1} and is associated with the stretching vibration of C-N. The binding of Zn with imidazole ligand induces the appearance of the bands at 765 cm^{-1} for Zn-O stretching and 422 cm^{-1} for Zn-N.[24,27-28] In the Fe$_3$O$_4$ spectra, the characteristic absorption band corresponding to Fe-O vibration was observed at 569 cm^{-1}, which is consistent with the reported literature.[29] The other band detected at 1,631 cm^{-1} correlates to the O-H deformed vibration, and at 3,319 cm^{-1} is correlated to the O-H stretching vibration of intermolecular bonded alcohol groups. Compared to parent components ZIF-8 and Fe$_3$O$_4$, the composite Fe$_3$O$_4$@ZIF-8 displays combined adsorption bands associated with the parent components. The bands correlated to Zn-O, Fe-O, and Zn-N metal nodes are observed at wavenumbers of 759, 567, and 425 cm^{-1}, respectively. The band correlated to C-N vibration was observed at 1,445 cm^{-1}, and the band appeared less intense than the ZIF-8 parent component. This functional group might interact with the Fe$_3$O$_4$ core to form the composite. The C = N vibration detected in the ZIF-8 spectrum disappears in the composite spectrum. The typical O-H stretching vibration band was observed at 3,475 cm^{-1}; this band is significantly shifted compared to the Fe$_3$O$_4$ spectrum.
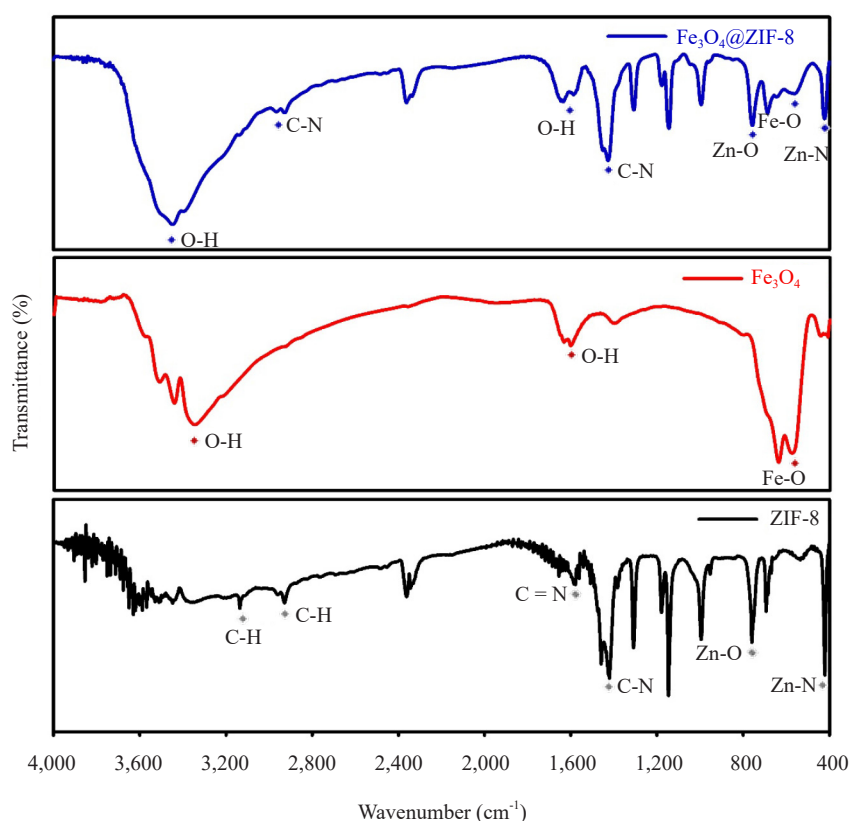
Figure 4. FTIR spectra of ZIF-8, Fe_3O_4, and Fe_3O_4@ZIF-8

3.3 *Adsorption kinetics*

The data points in Figure 5 depict the effect of varying the amount of GLYPi on time to reach the rapid, deceleration, and equilibrium adsorption stages. The rapid adsorption stage takes place over a longer period for higher adsorbate concentration; consequently, the deceleration and equilibrium stages start at a longer time. For example, adsorption of 20 mg/L GLYPi by Fe_3O_4@ZIF-8 requires 40 min to reach the equilibrium; meanwhile, it required 90 min and 120 min to reach equilibrium in adsorbing 40 and 60 mg/L of GLYPi respectively. This implies that a longer period was needed to adsorb a higher number of adsorbate. Furthermore, it can be noted that the adsorption capacity at a given time (Q_t) increases at higher adsorbate concentrations. This is because the concentration gradient difference between the bulk solution and the adsorbent surface becomes larger at higher adsorbate concentrations.[30]

The kinetic model fittings on the experimental data points were performed to quantitatively analyze the kinetics of GLYPi adsorption by ZIF-8 and Fe_3O_4@ZIF-8. Pseudo-first order (PFO), Pseudo-second order (PSO), and Elovich models were used for the data fittings. The mathematical expression of PFO, PSO, and Elovich is shown by eq. (4), (5), and (6), respectively.

$$Q_t = Q_{e1}\left(1 - e^{-k_1 t}\right) \qquad (4)$$

$$Q_t = Q_{e2}\left(\frac{Q_{e2} k_2 t}{1 + Q_{e2} k_2 t}\right) \qquad (5)$$

$$Q_t = \frac{1}{\beta}\ln(\alpha\beta) + \frac{1}{\beta}\ln t \tag{6}$$

where, Q_t (mg/g) is the adsorption capacity at a particular time (t, min). Q_{e1} (mg/g) and k_1 (1/min) is the PFO constant, which represents adsorption capacity and rate. Q_{e2} (mg/g) and k_2 (g/mg·min) is the adsorption capacity and rate according to PSO. The Elovich constant α describes the initial rate, and the constant β represents the desorption constant. The fitting results are depicted by the line curves in Figure 5a and 5b (for ZIF-8 and Fe$_3$O$_4$@ZIF-8, respectively); meanwhile, the derived constants and correlation coefficient (R^2) resulting from the fittings are summarized in Table 2. The adsorption kinetics behaviors of GLYPi by ZIF-8 and Fe$_3$O$_4$@ZIF-8 are best fitted by the PSO kinetic model, as indicated by greater R^2. This implies that chemisorption could be the rate-limiting factor in the system.[31] As derived from the PSO model, the adsorption rate (k_2) of GLYPi by ZIF-8 and Fe$_3$O$_4$@ZIF-8 was lower for the adsorption system with higher adsorbate concentration.

Table 2. Kinetics model parameters for GLYPi adsorption using ZIF-8 and Fe$_3$O$_4$@ZIF-8 as derived from PFO, PSO, Elovich, and ID model

Model	Parameter	GLYPi conc. (mg/L)		
		20	40	60
Adsorbent ZIF-8				
PFO	Q_{e1} (mg/g)	13.599	27.821	36.425
	k_1 (1/min)	0.0963	0.0724	0.0550
	R^2	0.9942	0.9901	0.9618
PSO	Q_{e2} (mg/g)	14.498	30.193	30.193
	k_2 (g/mg·min)	0.0107	0.0035	0.0035
	R^2	0.9983	0.9961	0.9961
Elovich	α (mg/g·min)	17.238	12.432	9.2104
	β (g/mg)	0.5124	0.2093	0.1278
	R^2	0.9318	0.9336	0.9554
ID	First segment			
	$C_{i,1}$ (mg/g)	-0.7265	-1.8132	-0.3504
	$k_{i,1}$ (mg/g·min$^{0.5}$)	2.7213	5.0182	5.5861
	R^2	0.9812	0.9660	0.9395
	Second segment			
	$C_{i,2}$ (mg/g)	8.7866	11.468	7.9362
	$k_{i,2}$ (mg/g·min$^{0.5}$)	0.6274	2.0334	3.3575
	R^2	0.9951	0.9986	0.9832
	Third segment			
	$C_{i,3}$ (mg/g)	13.645	27.155	35.197
	$k_{i,3}$ (mg/g·min$^{0.5}$)	0.0074	0.0744	0.1468
	R^2	0.4611	0.2511	0.5426

Table 2. (cont.)

Model	Parameter	GLYPi conc. (mg/L)		
		20	40	60
	Adsorbent composite Fe$_3$O$_4$@ZIF-8			
PFO	Q_{e1} (mg/g)	23.461	33.127	40.800
	k_1 (1/min)	0.0851	0.0503	0.0397
	R^2	0.9931	0.9837	0.9710
PSO	Q_{e2} (mg/g)	25.152	37.402	45.432
	k_2 (g/mg·min)	0.0055	0.0020	0.0012
	R^2	0.9937	0.9919	0.9853
Elovich	α (mg/g·min)	11.495	8.2522	6.2489
	β (g/mg)	0.3164	0.1666	0.1222
	R^2	0.9340	0.9582	0.9670
	First segment			
	$C_{i,1}$ (mg/g)	-1.1176	-0.1573	0.0820
	$k_{i,1}$ (mg/g·min$^{0.5}$)	2.5615	4.6914	5.4886
	R^2	0.9805	0.9906	0.9793
	Second segment			
	$C_{i,2}$ (mg/g)	14.397	11.108	4.7672
ID	$k_{i,2}$ (mg/g·min$^{0.5}$)	1.1524	2.5830	4.1360
	R^2	0.9756	0.9999	0.9933
	Third segment			
	$C_{i,3}$ (mg/g)	23.316	33.027	37.261
	$k_{i,3}$ (mg/g·min$^{0.5}$)	0.0305	0.0546	0.3197
	R^2	0.5065	0.5065	0.7594

Elovich model was originally derived to present a chemically-driven adsorption process.[32] The adsorption of GLYPi using ZIF-8 or Fe$_3$O$_4$@ZIF-8 was a chemisorption process, as it is more well correlated to the PSO than PFO. Thus, it is reasonable to evaluate the kinetic adsorption behavior further using the Elovich model. The adsorption rate of a chemisorption process is typically decreased with the increase of surface coverage, where the fractional unity of the surface coverage occurs faster at higher adsorbate concentration. This phenomenon can be well described from the constant α of the Elovich model, which represents the initial rate,[33-34] where the α value decreased with the increase of adsorbate concentration. It is worth noting that the initial adsorption rate was faster for ZIF-8 than Fe$_3$O$_4$@ZIF-8, as indicated by the higher α values. However, the desorption rate is lower from Fe$_3$O$_4$@ZIF-8 than ZIF, signified by lower β. Intraparticle diffusion (ID) model fitting was performed on the GLYPi adsorption data using ZIF-8 and Fe$_3$O$_4$@ZIF-8. ID fittings were performed on Q_t versus $t^{0.5}$ by employing eq. (7).

$$Q_t = C_{i,n} + k_{i,n}t^{0.5} \tag{7}$$

$C_{i,n}$ reflects the boundary layer effect, and $k_{i,n}$ represents the ID rate constant. As shown in Figure 6a and 6b (for ZIF-8 and Fe$_3$O$_4$@ZIF-8, respectively), the points of Q_t versus $t^{0.5}$ were not linear over the investigated time, suggesting that ID was not the sole rate-limiting factor. Two breakpoint times (t_{break}) are observed in the GLYPi adsorption using ZIF-8 and Fe$_3$O$_4$@ZIF-8, which divides the adsorption system into three rate-limiting mechanisms.[35-36] The first rate-limiting step, before the $t_{break,1}$, corresponds to the external diffusion. The second rate-limiting step, between $t_{break,1}$ and $t_{break,2}$, is driven by ID. After $t_{break,2}$, the third rate-limiting step correlates with the internal pore diffusion, which is a very slow (nearly constant) process. It can be noted that ZIF-8 has a faster external diffusion rate than Fe$_3$O$_4$@ZIF-8, as indicated by higher $k_{i,1}$. However, in the ID step, the Fe$_3$O$_4$@ZIF-8 shows a faster rate, implying that adding Fe$_3$O$_4$ enables the higher active sites. Furthermore, it was also noted that the $C_{i,n}$ values for Fe$_3$O$_4$@ZIF-8 in each step were larger than ZIF-8, indicating greater adsorption affinity.[37]

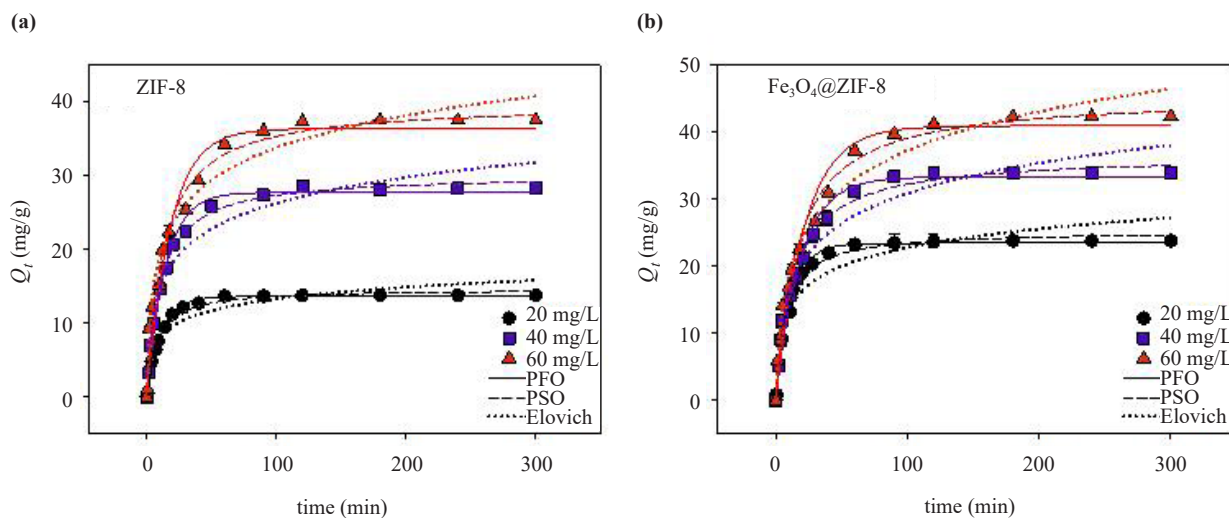**Figure 5.** Adsorption kinetics of GLYPi on (a) ZIF-8 and (b) Fe$_3$O$_4$@ZIF-8. The data points indicate the experimental measurements, and the lines indicate the kinetic model fittings (PFO, PSO, and Elovich)

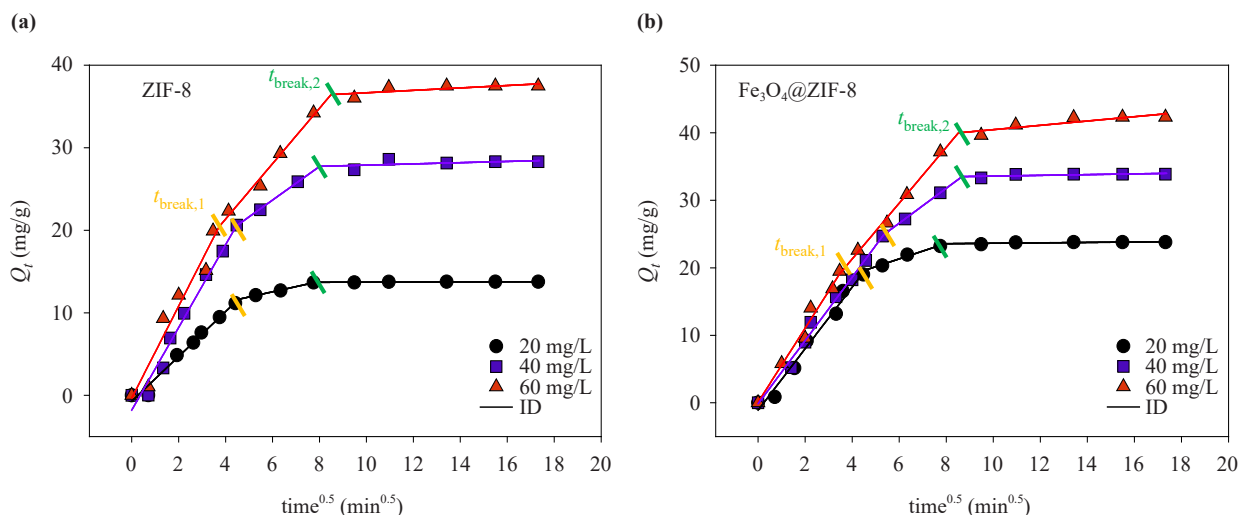**Figure 6.** Intraparticle diffusion (ID) model fitting on GLYPi adsorption using (a) ZIF-8 and (b) Fe$_3$O$_4$@ZIF-8

3.4 *Adsorption isotherm*

A batch adsorption experiment on a series of GLYPi at different concentrations (very low to adequately high) was conducted to find the maximum adsorption capacity. As shown in Figure 7, the adsorption isotherm of GLYPi on ZIF-8 or Fe$_3$O$_4$@ZIF-8 is in an L-class isotherm according to classification by Giles.[38] The adsorption sites of the adsorbent in this class tended to gradually diminish with an increasing adsorbate concentration, which was indicated by the presence of a plateau.[33] The investigated adsorption system of GLYPi can be further classified as subgroup two, which indicates the monolayer tendency of the system. The effect of temperature on the adsorption was also investigated. As shown in Figure 7, the equilibrium uptake of GLYPi by ZIF-8 and Fe$_3$O$_4$@ZIF-8 increased by increasing the temperature, suggesting the endothermic behavior of the adsorption process.
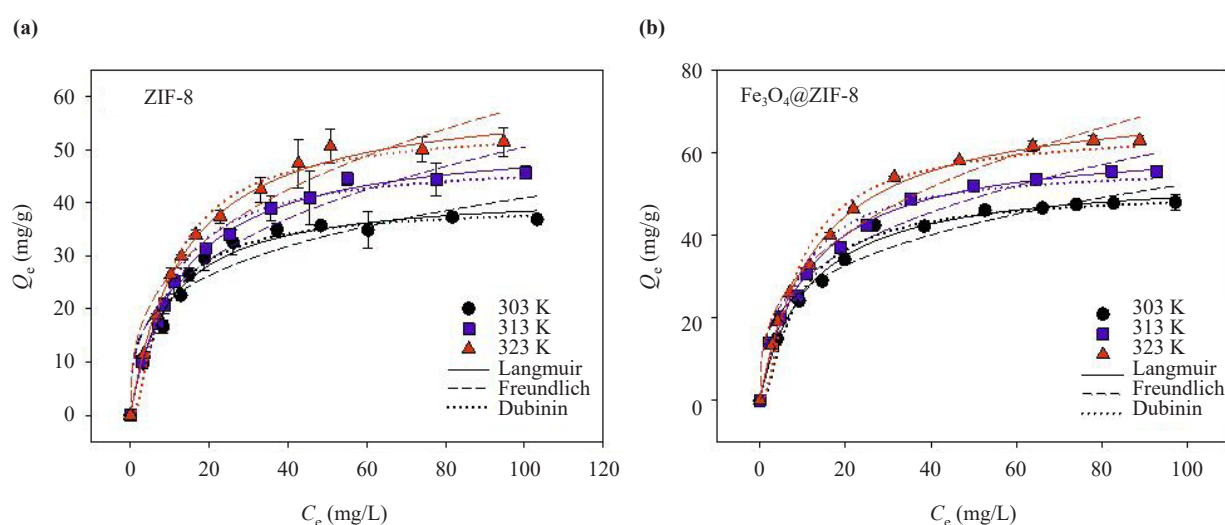

Figure 7. Adsorption isotherm of GLYPi on (a) ZIF-8 and (b) Fe$_3$O$_4$@ZIF-8. The data points indicate the experimental measurements, and the lines mark the isotherm model fittings

Two-parameter adsorption isotherm models were employed to quantitatively analyze the adsorption isotherm, that is, Langmuir, Freundlich, and Dubinin-Radushkevich model; their mathematical equations are shown by eq. (8), (9), and (10), respectively.

$$Q_e = Q_{L,max}\left(\frac{K_L C_e}{1 + K_L C_e}\right) \qquad (8)$$

$$Q_e = K_F C_e^{1/n_F} \qquad (9)$$

$$Q_e = Q_{DR,max} e^{-\left(K_{DR}\varepsilon^2\right)}, \text{ where } \varepsilon = RT\left(1 + \frac{1}{C_e}\right) \qquad (10)$$

where, Q_e (mg/g) and C_e (mg/L) are the adsorption capacity and sorbate concentration at equilibrium, respectively. $Q_{L,max}$ (mg/g) and K_L (L/mg) represent the Langmuir adsorption capacity and affinity. K_F (mg/g) is the Freundlich adsorption equilibrium constant, which correlated to the magnitude of surface heterogeneity (n_F, dimensionless). Similar to that of Langmuir constants, the Dubinin-Raduskevich $Q_{DR,max}$ (mg/g) and K_{DR} (L/mg) represent the maximum

adsorption capacity and affinity, respectively.

GLYPi adsorption isotherm model constants derived from several two- and three-parameter models

Model	Parameter	Temperature (K)		
		303	313	323
Adsorbent ZIF-8				
Langmuir	$Q_{L,max}$ (mg/g)	41.413	41.413	58.914
	K_L (L/mg)	0.0988	0.0988	0.0717
	R^2	0.9836	0.9836	0.9910
Freundlich	K_F (L/mg)	11.145	10.521	11.934
	n_F	3.7289	2.9876	2.9738
	R^2	0.9246	0.9469	0.9557
Dubinin-Radushkevich	$Q_{DR,max}$ (mg/g)	40.002	48.272	55.235
	$K_{DR} \times 10^2$ (kJ^2/mol^2)	1.2821	1.4658	1.4631
	E_{DR} (kJ/mol)	6.2449	5.8405	5.8458
	R^2	0.9829	0.9851	0.9870
Adsorbent composite Fe$_3$O$_4$@ZIF-8				
Langmuir	$Q_{L,max}$ (mg/g)	54.786	62.752	73.569
	K_L (L/mg)	0.0890	0.0876	0.0770
	R^2	0.9911	0.9917	0.9970
Freundlich	K_F (L/mg)	13.608	13.715	13.824
	n_F	3.4151	3.0720	2.8011
	R^2	0.9513	0.9702	0.9590
Dubinin-Randushkevich	$Q_{DR,max}$ (mg/g)	51.496	57.516	66.505
	$K_{DR} \times 10^2$ (kJ^2/mol^2)	1.3902	1.2583	1.3754
	E_{DR} (kJ/mol)	5.9972	6.3037	6.0294
	R^2	0.9831	0.9590	0.9778

The fitting curve is indicated by the line passing through the experimental data points in Figure 7, and the calculated constants derived from the models are listed in Table 3. A reasonable agreement was obtained between

the experimental data and the two-parameters Langmuir model, indicated by the highest R^2 value and the predicted maximum adsorption capacity ($Q_{J,max}$) value closest to the experimental result ($Q_{exp,max}$). The suitability of the GLYPi adsorption process with the Langmuir model suggests a homotattic behavior of the adsorbent,[39] which means that the adsorption sites possess homogeneous energy. The energy of GLYPi adsorption in aqueous phase can be calculated as E_{DR} (where, $E_{DR} = 1/\sqrt{2K_{DR}}$) parameter from the fitting using Dubinin-Raduskevich model.[40] It can be noted that ZIF-8 and Fe$_3$O$_4$@ZIF-8 have similar E_{DR} values of ~6 kJ/mol.

Thermodynamic analysis was performed on the adsorption isotherm data to evaluate (1) the spontaneity of the process based on the standard Gibb's free energy change $\Delta G°$ (kJ/mol), (2) the direction of energy transfer based on the enthalpy change $\Delta H°$ (kJ/mol), and (3) direction of the process based on the entropy change $\Delta S°$ (kJ/mol·K). The calculation of $\Delta G°$, $\Delta H°$, and $\Delta S°$ were performed using eqs. (11) to (12).

$$\Delta G^0 = -RT \ln K_C \tag{11}$$

$$\ln K_C = \frac{\Delta S^0}{R} - \frac{\Delta H}{RT} \tag{12}$$

where K_C value is obtained by multiplying the Jovanovich equilibrium constant (K_J, mg/L) with $Q_{J,max}$ (mg/g), and adsorbent concentration (A$_C$, g/L), according to eq. (13).

$$K_C = K_J \times Q_{J,\,max} \times A_C \tag{13}$$

R is the gas constant (8.314 J/mol·K), and T is the temperature (K). The values of $\Delta H°$ and $\Delta S°$ were calculated as the slope and intercept from the plot of K_C vs. $1/T$. The calculated thermodynamic parameters for the adsorption of GLYPi are listed in Table 4. The negative $\Delta G°$ value indicates the spontaneity of the adsorption process. The positive $\Delta H°$ confirms the endothermic behavior of the adsorption process. A positive $\Delta S°$ value indicates irreversible process behavior, which may be correlated to the difficulty of the adsorbate desorption.

Table 4. Thermodynamic parameter for adsorption of GLYPi by ZIF-8 and Fe$_3$O$_4$@ZIF-8

Parameter	ZIF-8			Fe$_3$O$_4$@ZIF-8		
	303 K	313 K	323 K	303 K	313 K	323 K
Regression eq.	$y = -520x + 9.6$			$y = -1150x + 11.7$		
$\Delta G°$ (kJ/mol)	-19.99	-20.66	-21.59	-19.93	-20.88	-21.88
$\Delta H°$ (kJ/mol)	4.32			9.57		
$\Delta S°$ (kJ/mol·K)	0.08			0.10		

3.5 *Effect of operating conditions on the adsorption performance*
3.5.1 *Effect of pH*

Figure 8 depicts the variation in the removal efficiency of GLYPi by ZIF-8 and Fe$_3$O$_4$@ZIF-8 under different pH. A gradual increase in removal efficiency can be observed with increasing pH, and this increasing trend continues until

the optimal value at pH 7 is reached. A dramatic decrease in removal efficiency then occurs at pH > 7. The ionization of GLYPi and the PZC of the adsorbent can explain the increasing and decreasing removal efficiency with respect to pH.[31] The ZIF-8 and Fe_3O_4@ZIF-8 adsorbents have a PZC of 8.8 (see results in Figure 1c), so they are positively charged at pH < 8.8. On the other hand, GLYPi molecules tend to become more negatively charged as the pH increases. Therefore, the electrostatic attraction force is expected to dominate and become stronger as the pH rises towards 8.8. Meanwhile, when the pH > 8.8, the adsorbent has a negative charge, causing a repulsive force and a decrease in removal efficiency. Furthermore, at pH > 8.8, the large number of hydroxyl anions in the solution can result in competition to occupy adsorption sites.
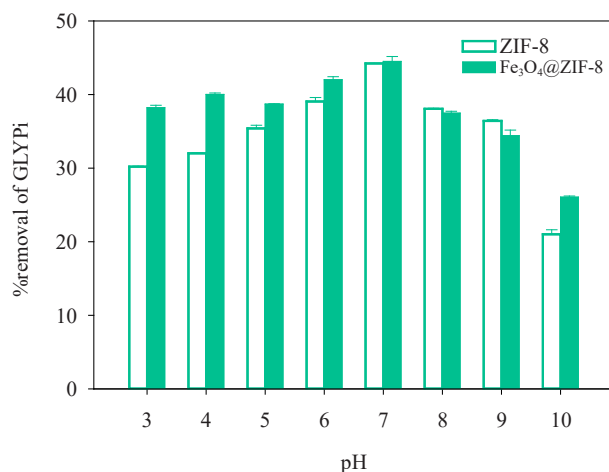

Figure 8. Removal of GLYPi by ZIF-8 and Fe_3O_4@ZIF-8 as the function of pH
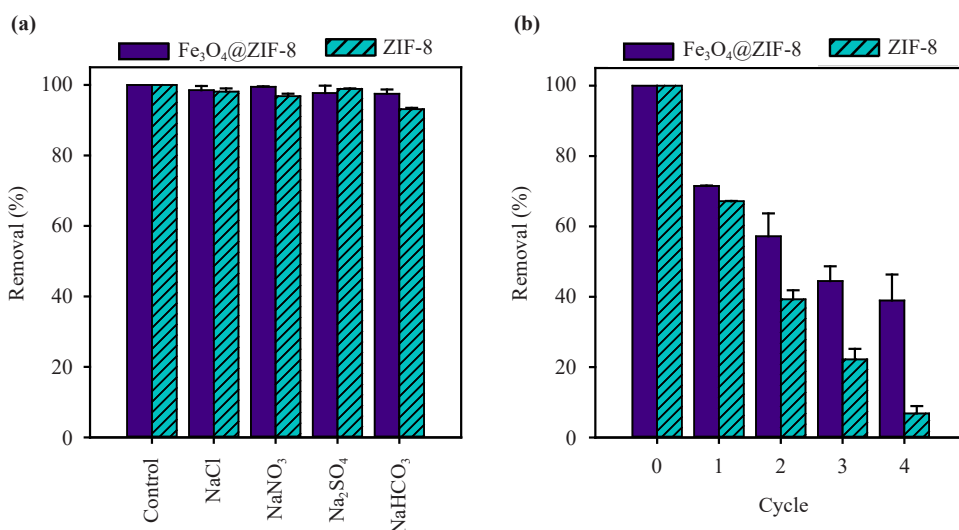
3.5.2 *Effect of salinity*

Figure 9. (a) Variation in the removal efficiency of GLYPi by ZIF-8 and Fe_3O_4@ZIF-8 under different salt background solutions. (b) Reusability of ZIF-8 and Fe_3O_4@ZIF-8 in 4 consecutive adsorption-desorption cycles

Salt with different types of anions was selected to investigate their effect on the removal efficiency of GLYPi by ZIF-8 and Fe$_3$O$_4$@ZIF-8. The effect of different cations was not considered in this work, as they would tend to repulse by the positively charged adsorbent; thus, their effect can be neglected. The effect of coexisting anion of Cl$^-$, SO$_4^{2-}$, NO$_3^-$, and HCO$_3^-$ on the removal efficiency of GLYPi is being investigated. It was expected that coexisting anions would compete with GLYPi for active adsorption (binding) sites of adsorbent, resulting in an inhibitive effect on the adsorption. However, based on the result in Figure 9a, it can be noted that the presence of coexisting anion does not significantly affect the removal efficiency of GLYPi by ZIF-8 and Fe$_3$O$_4$@ZIF-8. A possible explanation for this result is that there are still unsaturated sites after GLYPi adsorption; therefore, other anions only occupy these unsaturated adsorption sites.[41-42] Another possibility is that the adsorption of GLYPi by the adsorbent occurs via electrostatic interaction and physical interaction such as pore-filling.[43] Thus, the coexisting anions did not exhibit a significant reducing effect.

3.5.3 *Effect of repeated-cycle*

The ability to be used repeatedly can imply the economic aspect of an adsorbent. The adsorbent is regenerated through treatment with ethanol before being reused to release the adsorbed GLYPi molecules. In preliminary experiments, water was tested as a regenerating solvent. However, particles from adsorbents (especially ZIF-8) tend to float on the water, making separating difficult. Ethanol was chosen because of its non-toxic nature, and ethanol allows an easy separation process from the adsorbent via centrifugation. A previous pH effect study shows that the adsorption efficiency of GLYPi decreases drastically when the pH is highly alkaline. Therefore, to enable better release of the adsorbed GLYPi, NaOH was added to increase the pH of the solution. Figure 9b shows the variation in the removal efficiency of GLYPi by ZIF-8 and Fe$_3$O$_4$@ZIF-8 after undergoing several consecutive adsorption-desorption cycles. The results showed that the removal efficiency decreased significantly in the first cycle. The reduction in removal efficiency continues to occur for each cycle observed. This may be because the GLYPi molecule cannot be completely desorbed in each cycle; therefore, the un-desorbed GLYPi blocks the adsorption sites and pores of the adsorbent.

3.6 *Adsorption mechanism and comparison study*
3.6.1 *Mechanism*

The N$_2$ sorption isotherm curves of Fe$_3$O$_4$@ZIF-8 before and after adsorbing GLYPi are shown in Figure 10a. The Fe$_3$O$_4$@ZIF-8 exhibits a typical curve of a micro- and mesoporous material. Compared with before adsorption, the specific surface area (S_{BET}) of Fe$_3$O$_4$@ZIF-8 had decreased, which can be attributed to adsorbed GLYPi molecules blocking the pores of Fe$_3$O$_4$@ZIF-8. After adsorption, the total pore volume (V_p) was also slightly reduced for Fe$_3$O$_4$@ZIF-8. These results indicate that the adsorption of GLYPi on Fe$_3$O$_4$@ZIF-8 involves a pore-filling mechanism. The pore-filling mechanism in GLYPi adsorption has also been reported in a study by Jiang et al.,[43] where biochar-supported nano-zero-valent iron was used as the adsorbent.

The system pH was also revealed to affect the adsorption of GLYPi (see result in Figure 8). GLYPi possesses three deprotonable groups with a first dissociation constant (pKa_1) value of 2.2, pKa_2 of 5.5, and pKa_3 of 10.2, which corresponds to the deprotonation of H$^+$ at the carboxylic moiety and phosphonate moiety, respectively. The gradual increase in removal efficiency at pH 3-7 can be correlated with the increase in the negativity of the GLYPi molecule due to deprotonation of the carboxylate and phosphonate moieties. The increased negativity of GLYPi increases its attraction to the positively charged ZIF-8 and Fe$_3$O$_4$@ZIF-8; the attraction interaction between GLYPi and the adsorbent is illustrated in Figure 10b.
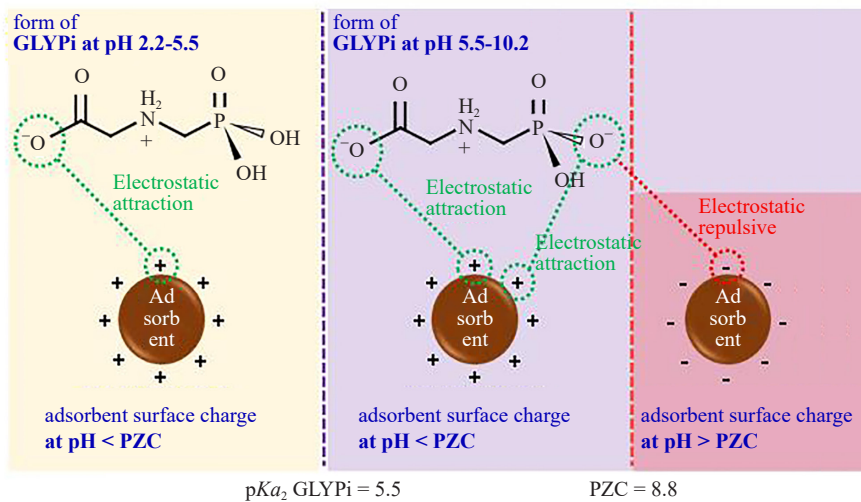
(a)
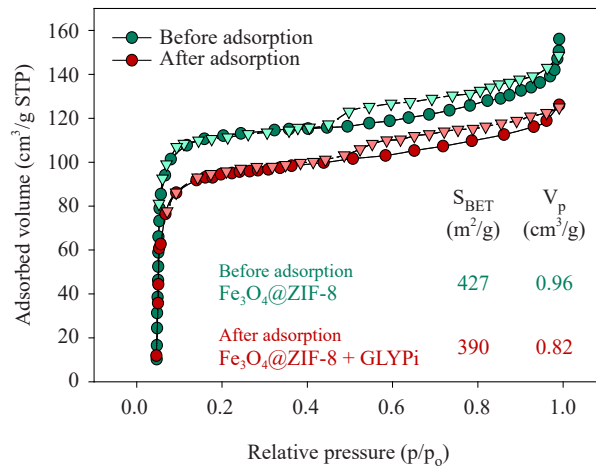
(b)

Figure 10. (a) N$_2$ sorption isotherm curve of Fe$_3$O$_4$@ZIF-8 before and after adsorbing GLYPi. (b) Electrostatic-driven interaction in GLYPi adsorption by Fe$_3$O$_4$@ZIF-8 at various pH ranges

3.6.2 Comparison of Fe$_3$O$_4$@ZIF-8 with other adsorbents for GLYPi adsorption

GLYPi has long been considered harmful to the environment, and its removal via the adsorption process has been widely reported in the literature. Evaluation of the adsorption capacity of GLYPi has been carried out using various adsorbent materials, ranging from natural to composite materials, as shown in Table 5. Natural-derived adsorbents (such as soil, biochar, and clay) exhibit low capacities for GLYPi adsorption compared to composite materials. The use of metal-organic frameworks (such as MIL-101 and MIL-125) exhibits significantly high GLYPi adsorption capacities, which is also higher than the Fe$_3$O$_4$@ZIF-8 composite in this study. However, comparing the solvent for synthesis and ease of separation, Fe$_3$O$_4$@ZIF-8 is still worth considering. In this case, water was used as the solvent for the synthesis, and the separation can be easily performed using an external magnetic field. Furthermore, Fe$_3$O$_4$@ZIF-8 also shows a moderate adsorption capacity of GLYPi.

Table 5. Comparison of GLYPi adsorption capacity with other adsorbents

Adsorbent*	pH	Temp. (°C)	Q_{max} (mg/g)	Ref.
Soil	5.9	20	21.4	44
Woody biochar	5.0	20	44.0	45
Palm biochar	4.0	25	40.49	43
PCH	8.0	50	27.5	46
MIL-101(Fe)	4.0	25	239.7	31
MIL-125(Ti)	5.4	25	128.0	47
BC-NZVI	4.0	25	80	43
MnFe$_2$O$_4$-G	4.7	25	39	48
GO-α-γ-Fe$_2$O$_3$	4.0 to 10.0	15	46.8	49
ZIF-8	7.0	30	41.41	This work
		40	50.21	
		50	58.91	
Fe$_3$O$_4$@ZIF-8	7.0	30	54.79	This work
		40	62.75	
		50	73.57	

* PCH = porous clay heterostructure; BC-NZVI = biochar modified with nano-zero-valent iron; MnFe$_2$O$_4$-G = reduced graphene oxide decorated with MnFe$_2$O$_4$ microsphere; GO-α-γ-Fe$_2$O$_3$ = α- and γ-Fe$_2$O$_3$ decorated graphene oxide

3.6.3 *Comparison of the adsorption performance for GLYPi and Pi*

Pi is an essential and irreplaceable element in agriculture; ~90% of world-mined Pi is used as fertilizer in various forms. The high usage of Pi-containing fertilizer has been stated to affect climate change negatively, and thus, a strategy for eliminating excess Pi in the environment is important. In this section, the adsorption performance of ZIF-8 and Fe$_3$O$_4$@ZIF-8 toward GLYPi is compared with the adsorption of Pi. Figure 11a compares the time needed for ZIF-8 and Fe$_3$O$_4$@ZIF-8 to adsorb between Pi and GLYPi. The adsorption of Pi proceeded faster than the adsorption of GLYPi. The equilibrium stage of Pi adsorption was able to reach within 20 min. Meanwhile, 40 min is required to achieve the equilibrium stage in the adsorption of GLYPi. The adsorption efficiency of Pi by ZIF-8 and Fe$_3$O$_4$@ZIF-8 is greater than GLYPi. It was found that 94% and 96% of Pi can be removed using ZIF-8 and Fe$_3$O$_4$@ZIF-8, and only 56% and 60% of GLYPi can be removed using ZIF-8 and Fe$_3$O$_4$@ZIF-8.

Figure 11b shows the experimental maximum adsorption capacity value for the adsorption of GLYPi and Pi. It can be noted that the adsorbents can adsorb Pi to a greater extent than GLYPi, which can be due to the structure of GLYPi being more complex and bulkier than Pi; thus, the adsorption process is hampered. Furthermore, it is worth noting that the modification of ZIF-8 with Fe$_3$O$_4$ does not synergistically improve the adsorption toward Pi. In contrast, the adsorption capacity toward GLYPi can be increased after modification of ZIF-8 with Fe$_3$O$_4$.
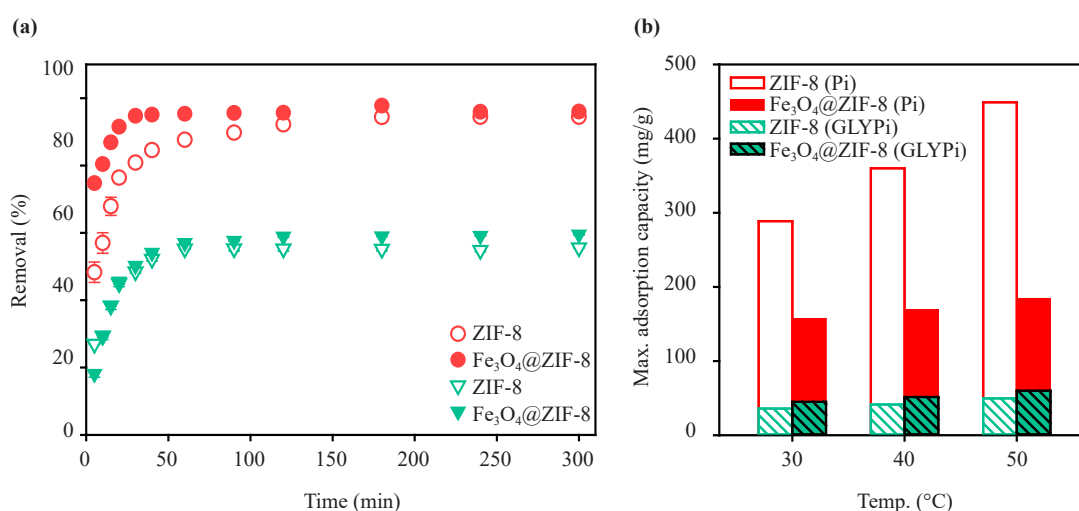
(a)

(b)

Figure 11. Comparison of ZIF-8 and Fe$_3$O$_4$@ZIF-8 for Pi (red) and GLYPi adsorption: (a) removal rate and (b) maximum adsorption capacity

4. Conclusion

Composite material constructs of Fe$_3$O$_4$ and ZIF-8 (Fe$_3$O$_4$@ZIF-8) were tested as adsorbents for removing GLYPi. The characterization results showed that the Fe$_3$O$_4$@ZIF-8 had rich oxygen-containing functional groups. The adsorption of GLYPi by Fe$_3$O$_4$@ZIF-8 was affected by contact time, solution pH, and repeated cycles. The adsorption kinetic analysis revealed the suitability of PSO in modeling the data, and the ID model indicated that the adsorption is controlled by external diffusion, internal pore diffusion, and intraparticle diffusion. The adsorption isotherm data correlated well with the Langmuir model, and the maximum GLYPi adsorption capacity of Fe$_3$O$_4$@ZIF-8 composite was 73.57 mg/g, which is higher than ZIF-8 (58.91 mg/g). The coexisting anion pollutants have a minimum influence on the adsorption of GLYpi by Fe$_3$O$_4$@ZIF-8. The adsorption process involves mechanisms, including pore-filling and electrostatic interaction. For comparison purposes, the adsorption of Pi was also investigated, and the Fe$_3$O$_4$@ZIF-8 composite showed an excellent adsorption performance toward Pi with a maximum adsorption capacity three times higher than GLYPi. The higher affinity of Fe$_3$O$_4$@ZIF-8 toward Pi may lead to reduced adsorption sites toward Pi, which may adversely affect the adsorption of GLYPi. Overall, this study demonstrated that the Fe$_3$O$_4$@ZIF-8 composite is an effective candidate for the adsorption of Pi-containing compounds, which can be an excellent option for environmental cleaning.

Author contribution statement

J. O. Ondang-Writing-Original draft preparation, Investigation, Formal analysis. A. E. Angkawijaya & A. W. Go-Writing-Original draft preparation, Investigation, Resources. F. E. Soetaredjo & S. Ismadji-Methodology, Validation. H. Y. Hsu, K.C. Cheng, & C. W. Hsieh-Project administration. P. L. Tran-Nguyen-Writing-Review & Editing. S. P. Santoso-Writing-Review & .Editing, Conceptualization, Funding acquisition.

Acknowledgment

Conflict of interest

The authors declare that they have no known competing financial interests or personal relationships that could have appeared to influence the work reported in this paper.

References

[1] Soares, D.; Silva, L.; Duarte, S.; Pena, A.; Pereira, A. *Foods* **2021**, *10*, 2785.

[2] Baer, K. N.; Marcel, B. J., Glyphosate. In *Reference Module in Biomedical Sciences: Encyclopedia of Toxicology*; Wexler, P., Ed.; Elsevier: Academic Press, 2014; pp 767-769.

[3] Bai, S. H.; Ogbourne, S. M. *Environ. Sci. Pollut. Res.* **2016**, *23*, 18988-19001.

[4] Martins-Gomes, C.; Silva, T. L.; Andreani, T.; Silva, A. M. *J. Xenobiotics* **2022**, *12*, 21-40.

[5] Hébert, M.-P.; Fugère, V.; Gonzalez, A. *Front. Ecol. Environ.* **2018,** *17*, 48-56.

[6] Richmond, M. E. *J. Environ. Stud. Sci.* **2018,** *8*, 416-434.

[7] Ruano, G.; Pedano, M. L.; Albornoz, M.; Fuhr, J. D.; Martiarena, M. L.; Zampieri, G. *Appl. Surf. Sci.* **2021**, *567*, 150753.

[8] Kanissery, R.; Gairhe, B.; Kadyampakeni, D.; Batuman, O.; Alferez, F. *Plants (Basel)* **2019**, *8*, 499.

[9] Solomon, K. R.; Thompson, D. G. *J .Toxicol. Environ. Health B. Crit. Rev.* **2003**, *6*, 289-324.

[10] Li, J.; Chang, H.; Li, Y.; Li, Q.; Shen, K.; Yi, H.; Zhang, J. *RSC Adv.* **2020**, *10*, 3380-3390.

[11] Sen, K.; Chattoraj, S., A comprehensive review of glyphosate adsorption with factors influencing mechanism: Kinetics, isotherms, thermodynamics study. In *Intelligent Environmental Data Monitoring for Pollution Management: Intelligent Data-Centric Systems*; Bhattacharyya, S., Platos, J., Krömer, P., Mondal, N. K., Snášel, V., Eds.; Elsevier: Academic Press, 2021; pp 93-125.

[12] Oh, S.; Lee, S.; Lee, G.; Oh, M. *Sci. Rep.* **2023**, *13*, 12250.

[13] Huang, C.; Zhang, H.; Zheng, K.; Zhang, Z.; Jiang, Q.; Li, J. *Sci. Total Env.* **2021**, *785*, 147382.

[14] Liu, J.; Li, J.; Wang, G.; Yang, W.; Yang, J.; Liu, Y. *J. Colloid Interface Sci.* **2019**, *555*, 234-244.

[15] Begum, J.; Hussain, Z.; Noor, T. *Mater. Res. Express* **2020**, *7*, 015083.

[16] Pearson, R. G. *Surv. Prog. Chem.* **1969**, *5*, 1-52.

[17] Reed, J. L. *Inorg. Chem.* **2008**, *47*, 5591-5600.

[18] Alvares, E.; Tantoro, S.; Wijaya, C. J.; Cheng, K.-C.; Soetaredjo, F. E.; Hsu, H.-Y.; Angkawijaya, A. E.; Go, A. W.; Hsieh, C.-W.; Santoso, S. P. *Int. J. Bio. Macromol.* **2023**, *231*, 123322.

[19] Jian, M.; Liu, B.; Liu, R.; Qu, J.; Wang, H.; Zhang, X. *RSC Adv.* **2015**, *5*, 48433-48441.

[20] Kosmulski, M. *Adv. Colloid Interface Sci.* **2023**, *319*, 102973.

[21] Hamza, M. F.; Guibal, E.; Wei, Y.; Ning, S. *Chem. Eng. J.* **2023**, *464*, 142638.

[22] Lunardi, V. B.; Cheng, K.-C.; Lin, S.-P.; Angkawijaya, A. E.; Go, A. W.; Soetaredjo, F. E.; Ismadji, S.; Hsu, H.-Y.; Hsieh, C.-W.; Santoso, S. P. *J. Hazard. Mater.* **2024**, *464*, 132973.

[23] Kosmulski, M. *Adv. Colloid and Interface Sci.* **2021**, *296*, 102519.

[24] Guo, Z.; Li, W.; Li, W.; Hou, X.; Luan, S.; Song, Y.; Wang, Q. *Microporous Mesoporous Mater.* **2021**, *310*, 110677.

[25] Schejn, A.; Aboulaich, A.; Balan, L.; Falk, V.; Lalevée, J.; Medjahdi, G.; Aranda, L.; Mozeta, K.; Schneider, R. *Catal. Sci. Technol.* **2015**, *5*, 1829.

[26] Lee, Y.-R.; Jang, M.-S.; Cho, H.-Y.; Kwon, H.-J.; Kim, S.; Ahn, W.-S. *Chem. Eng. J.* **2015**, *271*, 276-280.

[27] Liu, J.; He, J.; Wang, L.; Li, R.; Chen, P.; Rao, X.; Deng, L.; Rong, L.; Lei, J. *Sci. Rep.* **2016**, *6*, 23667.

[28] Zhang, T.; Zhang, X.; Yan, X.; Kong, L.; Zhang, G.; Liu, H.; Qiu, J.; Yeung, K. L. *Chem. Eng. J.* **2013**, *228*, 398-404.

[29] Ta, T. K. H.; Trinh, M.-T.; Long, N. V.; Nguyen, T. T. M.; Nguyen, T. L. T.; Thuoc, T. L.; Phan, B. T.; Mott, D.; Maenosono, S.; Tran-Van, H.; Le, V. H. *Colloids Surf. A Physicochem. Eng. Asp.* **2016**, *504*, 1-8.

[30] Pourhakkak, P.; Taghizadeh, A.; Taghizadeh, M.; Ghaedi, M.; Haghdoust, S., Fundamentals of adsorption technology. In *Adsorption: Fundamental Processes and Applications*; Ghaedi, M., Ed.; Elsevier: Academic Press, 2021; pp 1-70.

[31] Liu, R.; Xie, Y.; Cui, K.; Xie, J.; Zhang, Y.; Huang, Y. *J. Phys. Chem. Solids* **2022**, *161*, 110403.

[32] Largitte, L.; Pasquier, R. *Chem. Eng. Res. Des.* **2016**, *109*, 495-504.

[33] Ghavamifar, S.; Naidu, R.; Mozafari, V.; Li, Z. *Chemosphere* **2023**, *311*, 136922.

[34] Wu, F.-C.; Tseng, R.-L.; Juang, R.-S. *Chem. Eng. J.* **2009**, *150*, 366-373.

[35] Wang, J.; Guo, X. *Chemosphere* **2022,** *309*, 136732.

[36] Teixeira, R. N. P.; Neto, V. O. S.; Oliveira, J. T.; Oliveira, T. C.; Melo, D. Q.; Silva, M. A. A.; Nascimento, R. F. *Bioresources* **2013,** *8*, 3556-3573.

[37] Pholosi, A.; Naidoo, E. B.; Ofomaja, A. E. *S. Afr. J. Chem. Eng.* **2020,** *32*, 39-55.

[38] Giles, C. H.; Smith, D.; Huitson, A. *J. Colloid Interface Sci.* **1974,** *47*, 755-765.

[39] Al-Ghouti, M. A.; Da'ana, D. A. *J. Hazard. Mater.* **2020,** *393*, 122383.

[40] Mudhoo, A.; Pittman Jr., C. U. *Chem. Eng. Res. Des.* **2023,** *198*, 370-402.

[41] Barnie, S.; Zhang, J.; Wang, H.; Yin, H.; Chen, H. *Chemosphere* **2018,** *212*, 209-218.

[42] Liang, C.; Wu, H.; Chen, J.; Wei, Y. *Ecotoxicol. Environ. Saf.* **2023,** *249*, 114474.

[43] Jiang, X.; Ouyang, Z.; Zhang, Z.; Yang, C.; Li, X.; Dang, Z.; Wu, P. *Colloids Surf. A Physicochem. Eng. Asp.* **2018,** *547*, 64-72.

[44] Gimsing, A. L.; Szilas, C.; Borggaard, O. K. *Geoderma* **2007,** *138*, 127-132.

[45] Mayakaduwa, S. S.; Kumarathilaka, P.; Herath, I.; Ahmad, M.; Al-Wabel, M.; Ok, Y. S.; Usman, A.; Abduljabbar, A.; Vithanage, M. *Chemosphere* **2016,** *144*, 2516-2521.

[46] Besghaier, S.; Cecilia, J. A.; Chouikhi, N.; Vilarrasa-García, E.; Rodríguez-Castellón, E.; Chlendi, M.; Bagane, M. *Braz. J. Chem. Eng.* **2022,** *39*, 903-917.

[47] Naghdi, S.; Brown, E.; Zendehbad, M.; Duong, A.; Ipsmiller, W.; Biswas, S.; Toroker, M. C.; Kazemian, H.; Eder, D. *Adv. Funct. Mater.* **2023,** *33*, 2213862.

[48] Yamaguchi, N. U.; Bergamasco, R.; Hamoudi, S. *Chem. Eng. J.* **2016,** *295*, 391-402.

[49] Santos, T. R. T.; Andrade, M. B.; Silva, M. F.; Bergamasco, R.; Hamoudi, S. *Environ. Technol.* **2019,** *40*, 1118-1137.